Advances in Science and Technology Research Journal

Advances in Science and Technology Research Journal, 2026, 20(6), 381–402
https://doi.org/10.12913/22998624/218517
ISSN 2299-8624, License CC-BY 4.0

Received: 2025.12.24
Accepted: 2026.04.15
Published: 2026.05.01

Effect of longitudinal stiffener geometry and stiffener parameters on the buckling behavior of thin-walled stainless steel 304 cylindrical columns under axial compression

Saif Imad Abdualrazak[1], I.A. Abdulsahib[1], Hussein M. H. Al-Khafaji [1]

[1] College of Mechanical Engineering, University of Technology, Baghdad, Iraq
* Corresponding author's e-mail: saif.im.abdualrazak@uotechnology.edu.iq

ABSTRACT

Longitudinal stiffeners are commonly used in engineering practice to enhance the strength and buckling resistance. This study examines the effects of three stiffener geometries (I-, L-, and U-shaped) under equal-mass conditions to quantify the influence of longitudinal stiffener geometry on the buckling behavior of thin-walled SS304 cylindrical columns. To evaluate their influence on the buckling response, following factors were chosen: stiffener shape, number of longitudinal stiffeners (Ns), stiffener circumferential spacing ratio (p_w/s), and stiffener width-to-stiffener thickness ratio (b/ts). An experimental program was conducted to validate the finite element simulation. Nonlinear finite element simulations were applied using Abaqus. The finite element output was analyzed using the Taguchi method to identify the best parameter combinations for highest buckling strength. The analysis of variance (ANOVA) method was utilized to determine the influence of each parameter on the critical buckling load. The outcomes indicated that the combination of parameters exhibiting the greatest buckling resistance corresponds to the U-shaped stiffener configuration with several longitudinal stiffeners (Ns = 6), stiffener width-to-stiffener thickness ratio (b/ts = 2.2), and a circumferential spacing ratio (p_w/s = 0.6). The results further indicated the number of stiffeners and their circumferential spacing are the most influential factors for buckling resistance, and stiffener width-to-stiffener thickness ratio is the least influential.

Keywords: thin-walled cylindrical columns, longitudinal stiffeners, buckling behavior, axial compression, stiffener geometry, circumferential spacing ratio, stiffener width-to-stiffener thickness ratio, stainless steel.

INTRODUCTION

Thin-walled cylindrical columns are widely used in modern lightweight structures due to their high strength-to-weight efficiency; however, they are extremely sensitive to buckling and premature failure under axial compression, particularly when unstiffened, where even small geometric imperfections or unfavorable boundary conditions may trigger sudden collapse and significant economic losses. Consequently, stiffening structural has become an essential engineering strategy to enhance buckling resistance and ensure structural safety. Longitudinal stiffeners are a common way to make structures more stable and less likely to fail, but their effectiveness depends on many factors, such as the shape of the stiffener, the number of stiffeners, the circumferential spacing, the details of the attachment, and the thickness of the stiffener. The fundamental behavior of thin-walled cylindrical columns has been extensively investigated since the pioneering work of NASA [1], which established a comprehensive framework for elastic and inelastic buckling through the SP-8007 report and introduced knockdown factors that remain a global reference for shell design. This theoretical foundation was further formalized [2], who clarified elastic stability equations and boundary condition modeling. Subsequent studies highlighted the pronounced sensitivity of cylindrical shells to geometric imperfections, where [3] demonstrated that even minor deviations can significantly

reduce the critical buckling load, while nonlinear finite element investigations by [4] confirmed that geometric imperfections and residual stresses exert a dominant influence on buckling behavior. Later developments [5] showed that post-buckling response follows a gradual nonlinear stiffness degradation rather than an abrupt loss of load-carrying capacity. With the introduction of stiffening systems, experimental and numerical investigations [6,7] demonstrated that increasing the number of longitudinal stiffeners can suppress local buckling and alter post-buckling load redistribution, although the resulting increase in critical load is not necessarily linear. Furthermore, showed that stiffener geometry plays a decisive role in balancing stiffness enhancement and post-buckling stability [8], as different profiles activate distinct deformation and load-transfer mechanisms. In addition to elastic and nonlinear buckling, experimental investigations on axially compressed circular tubes conducted [9] demonstrated that thin-walled columns may undergo localized plastic deformation prior to global collapse, highlighting the importance of considering plastic buckling mechanisms in nonlinear stability analyses, particularly for ductile materials such as stainless steel. Beyond global geometry, the effectiveness of stiffened thin-walled members has been shown to be strongly influenced by connection detailing and load-transfer efficiency between the stiffener and the shell. Reported that shear-lag effects and insufficient weld stiffness may limit composite action and reduce buckling efficiency. In this context [10], demonstrated that resistance spot welding parameters significantly affect local stiffness, failure initiation [11], and load-transfer efficiency in cold-formed steel members, indicating that even optimized stiffener geometry may not be fully activated without adequate and sufficiently stiff attachment. Nonlinear local and global buckling behavior of thin-walled steel columns is also highly sensitive to geometric imperfections and material nonlinearity. Showed that plastic buckling of stainless-steel cylindrical shells is strongly influenced by material nonlinearity and imperfection sensitivity under axial compression [12], emphasizing the importance of nonlinear constitutive modeling for stainless-steel columns. Independently, demonstrated that although imperfection amplitude affects the absolute buckling load [13], comparative trends between different geometrical configurations remain relatively stable, supporting the use of eigenmode-based imperfection modeling in nonlinear parametric studies. Furthermore, hybrid experimental–numerical frameworks validated against representative experiments have been shown to reliably capture structural trends and parametric sensitivity beyond the experimentally tested cases. In this regard, confirmed that once a nonlinear finite element model is experimentally verified, it can be confidently extended to investigate a wider parametric space [14]. Regional experimental investigations conducted [15] likewise confirmed that realistic boundary conditions and appropriate stiffening significantly enhance the buckling resistance of thin-walled steel members. Parallel to mechanical investigations, statistical optimization techniques have been increasingly applied to buckling problems, demonstrated that Taguchi and ANOVA-based approaches can identify dominant geometric ratios governing the buckling response of longitudinally stiffened cylindrical columns [16–18].

This study focuses on stainless-steel columns under axial compression, particularly because of their importance in engineering applications that require both lightweight structural efficiency and effective buckling resistance. Despite notable advancements in the literature, existing studies often vary stiffener geometry without accounting for mass equality or examine individual parameters in isolation. A clear research gap remains regarding the combined influence of stiffener shape, number, rigidity, and circumferential stiffener distribution when the stiffeners are constrained to equal mass. The equal-mass stiffener concept is adopted as a rational normalization strategy to isolate the influence of stiffener geometry while eliminating weight as a confounding variable, which is particularly relevant in early-stage structural optimization where a fixed material budget is redistributed rather than increased. Accordingly, the equal-mass approach employed in this study serves as a comparative and optimization-oriented framework rather than a direct fabrication or cost-equivalence prescription. In response to this gap, the present work focuses on comparing three stiffener geometries I-shaped, L-shaped, and U-shaped profiles through a systematic evaluation of key parameters: stiffener geometry, the number of stiffeners (Ns), the stiffener width-to-thickness ratio (b/ts), and the circumferential spacing ratio (p_w/s). This work investigates the effect of variations in these parameters on the buckling behavior of

thin-walled cylindrical columns made of SS304 stainless steel under axial loading, with the primary objective of quantifying the influence of stiffener geometry on buckling resistance under equal-mass conditions.

THEORY

Buckling and finite element

Buckling is a state of a structure in which the applied loads are large enough to disturb or destroy its stability. The linear analysis of buckling determines its theoretical strength. It is modeled as an eigenvalue equation:

$$(k + \lambda k\sigma)/\psi = 0 \quad (1)$$

where: $k\sigma$ is a stress-stiffness matrix, λ is the eigenvalue (load factor), k is the stiffness matrix, and ψ is the eigenvector of displacements.

The outcomes for this formula are the eigenvalues and corresponding eigenvectors. The smallest value from the eigenvalues represents the critical load factor of buckling. If the applied load is (P), then the critical load will be (λ*P). If the load is pure bending and the cross-section of the structure is uniform, there will be both positive and negative factors for load, but they have equal absolute values. Therefore, the critical load factor must be determined based on the direction of the applied load [19,20].

Nonlinear buckling analysis

Nonlinear buckling analysis gives a greater accuracy than elastic formulation. This analysis is a static method, which concerns a nonlinearity of materials and geometrics, and boundaries' nonlinearity. In this type of analysis, the load is applied gradually until a small increment of the load makes a big change in displacement; at this point, the state of the structure becomes unstable, and the load represents the critical buckling load [21]. This study used the nonlinear analysis because it is close to the real behaviour of the structure.

Taguchi

Genichi Taguchi established the Taguchi technique in 1949. It is a mechanism for determining the link between the input process and the output of products. The outcome relies on employing an orthogonal array (OA) with a limited number of tests to identify the optimal set of parameters for the procedure. This method serves as an effective instrument for enhancing design by integrating the principles of quality loss function and design of experiments theory. It offers a methodical strategy for enhancing design efficacy, expense, and excellence. Furthermore, the method utilizes a statistical metric known as the signal-to-noise ratio (S/N), which is defined as the ratio of the mean (signal) to the standard deviation (noise), representing a logarithmic function of the desired output. There are three conventional classifications of signal-to-noise ratio: greater the best (HB), lower the best (LB), and nominal the better (NB) [22–24]. In this investigation, a greater buckling strength is necessitated; hence, a superior formula is employed.

$$S/N = -10\,log\,(\tfrac{1}{n}\textstyle\sum_{i=1}^{n}\frac{1}{y^2}) \quad (2)$$

where: y represents the read data, and n is the observations' number.

ANALYSIS OF VARIANCE

Analysis of variance (ANOVA) is an effective statistical method that identifies significant factors and illustrates the percentage contribution of each parameter. This research employed the signal-to-noise ratio (S/N) for decision-making. The ANOVA technique relies on the total sum of squared deviations (SS_T), which is represented as [25]:

$$SS_T = \textstyle\sum_{(i=1)}^{(n)} (n_i - n_m)^2 \quad (3)$$

The percentage of contribution (P) could be calculated as:

$$P = \frac{SS_d}{SS_T} \quad (4)$$

$$\begin{matrix} d.o.f\ of\ any\ parameter(factor)\ = k-1 \\ Total\ d.o.f\ = n-1 \end{matrix} \quad (5)$$

$$Total\ d.o.f\ = n-1 \quad (6)$$

$$d.o.f\ of\ error\ = \\ = total\ d.o.f - \sum d.o.f\ of\ parameters \quad (7)$$

$$V = \frac{SS_d}{d.o.f} \quad (8)$$

$$F = \frac{V}{V_E} \quad (9)$$

where: n is the number of trails (observation) in the orthogonal array, n_i is mean of S/N ratio for the observation, n_m is mean of all parameters, SS_d is a summation of the squared deviations, k is levels' number for each parameter, P is contribution's percentage, V is parameter's factor variance, V_E is error's variance, $d.o.f$ is the degree of freedom, and, F is the F-value (test statistic) used in ANOVA to evaluate the statistical significance of each factor.

Specimen geometry design

The specimens are designed to represent thin-walled cylindrical columns with longitudinal stiffeners, reflecting the geometry and cross-sectional boundary conditions of thin-walled (D/t = 125) structural components. Each specimen consists of a stainless-steel cylindrical column with a constant wall (D = 100 mm) thickness (t = 0.8 mm) and length (L = 590 mm). Dimensions are shown in Figure 1, particularly in Figures 1a, 1b, and 1c, dimensions of the specimen designed according to Eurocode [26]. In line with previous experimental studies on thin-walled spot-welded structures, where a weld spacing (p_w = 30 mm) was adopted for sheet joints to ensure stable load transfer and minimize shear lag effects [27].

Table 1 shows the dimensions of the longitudinal stiffeners on which the simulation will be performed. The distribution of these dimensions ensures that the shapes are of equal mass (92 g) per stiffener (I-, L-, and U-shaped) and a cross-sectional area of approximately 16 mm². The circumferential spacing (s) for all stiffener shapes depends on the number of longitudinal stiffeners (Ns) and the cylinder circumference, resulting in values of (s = 157, 78.5, and 52.3 mm) for (Ns = 2, 4, and 6), respectively.

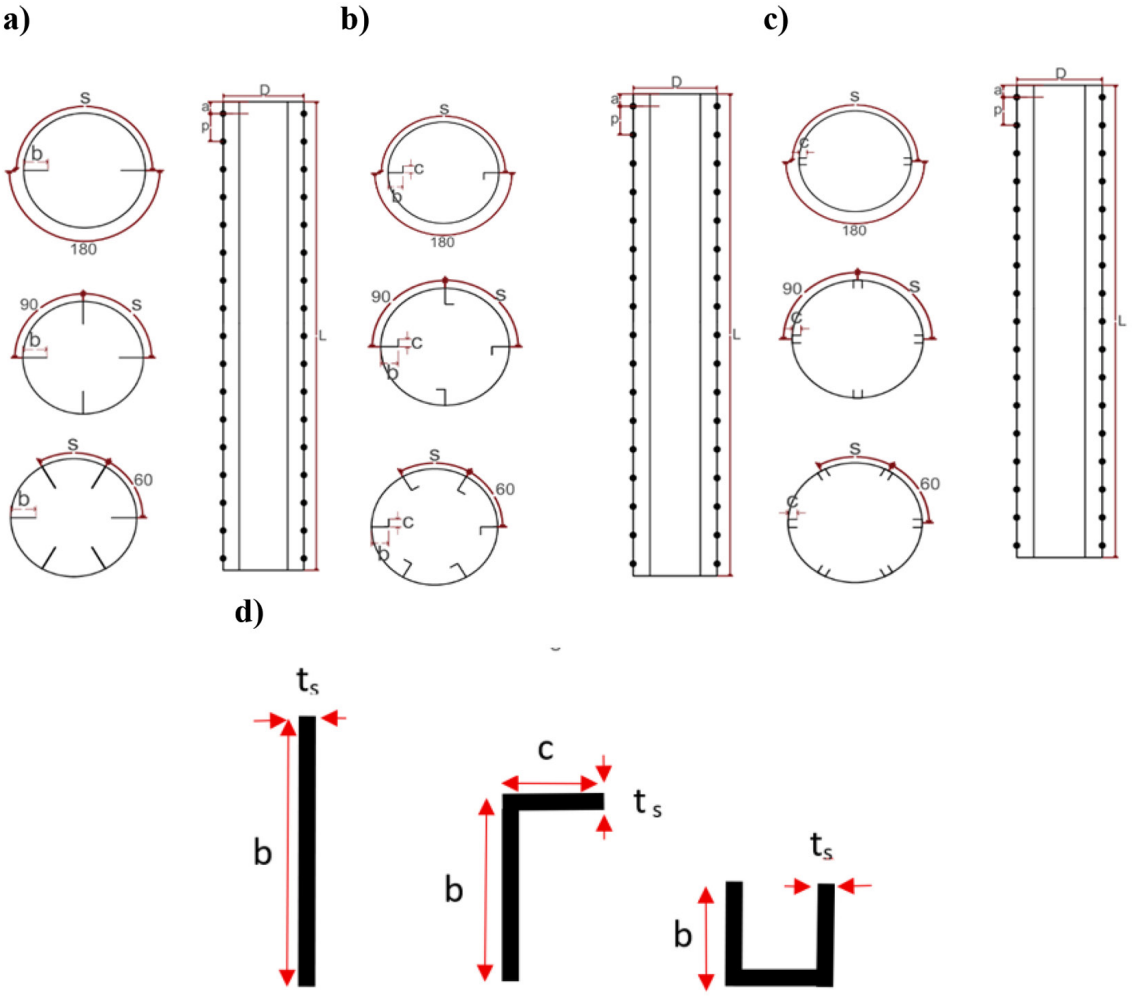

Figure 1. Specimen dimensions (a) I-shape stiffener; (b) L-shape stiffener; (c) U-shape stiffener; (d) the dimensions of the longitudinal stiffeners

Table 1. Geometric dimensions of longitudinal stiffeners under equal-mass conditions

Number of stiffeners (Ns)	Shape of stiffener	Thickness of stiffener (ts) (mm)	High stiffeners (b) (mm)	Edge of stiffener (c) (mm)
2,4,6	I	0.8	20	0
2,4,6	I	1.6	10	0
2,4,6	I	2.4	7	0
2,4,6	L	0.8	13.5	6.5
2,4,6	L	1.6	7	3
2,4,6	L	2.4	5	2
2,4,6	U	0.8	7	7
2,4,6	U	1.6	3.5	3.5
2,4,6	U	2.4	2.2	-

EXPERIMENTAL PROGRAM

The objective of the experimental program is to study the influence of the longitudinal stiffener geometry on the buckling behaviour of thin-walled SS304 cylindrical columns. Each stiffener shape was applied in configurations of 2, 4, and 6 stiffeners with thicknesses of stiffener (ts) of 0.8 mm, 1.6 mm, and 2.4 mm, producing 27 specimens. Table 2 summarizes the parameters according to the stiffener-geometry criterion: the number of stiffeners (Ns), stiffener width-to-stiffener thickness ratio (b/ts), and the circumferential spacing ratio (p_w/s), enabling a direct comparison of the structural efficiency of the I-, L-, and U-shape stiffeners.

Manufacturing and welding process

The product manufacturing process involved three steps: cutting, rolling, and welding, as illustrated in Figure 2. All welding parameters, such as wire type, weld circle diameter, and spacing, were carefully and scientifically recorded to ensure repeatability and quality control. Initially, a CNC laser cutting machine (A fiber laser) is applied in cutting metal sheets with nitrogen at an initial operating pressure of p being, 24 bars. Such high operating nitrogen pressure facilitates high-quality cuts [28] was used to cut the pieces in a dedicated workshop, as shown in Figure 2(a), were rolled into a circle to match the desired sample shape and achieve the desired cylindrical

Table 2. Selected parameters and levels for the I-shaped stiffener geometry: number of longitudinal stiffeners (Ns), stiffener width-to-thickness ratio (b/ts), and circumferential spacing ratio (p_w/s); Selected parameters and levels for the L-shaped stiffener geometry: number of longitudinal stiffeners (Ns), stiffener width-to-thickness ratio (b/ts), and circumferential spacing ratio (p_w/s); Selected parameters and levels for the U-shaped stiffener geometry: number of longitudinal stiffeners (Ns), stiffener width-to-thickness ratio (b/ts), and circumferential spacing ratio (p_w/s)

Selected parameters and levels for the I-shaped stiffener geometry				
Symbols	Parameter	Level 1	Level 2	Level 3
A	Ns	2	4	6
B	b/ts	25	6.25	2.9
C	p_w/s	0.2	0.4	0.6
Selected parameters and levels for the L-shaped stiffener geometry				
Symbols	Parameter	Level 1	Level 2	Level 3
A	Ns	2	4	6
B	b/ts	16.6	4.3	2
C	p_w/s	0.2	0.4	0.6
Selected parameters and levels for the U-shaped stiffener geometry				
Symbols	Parameter	Level 1	Level 2	Level 3
A	Ns	2	4	6
B	b/ts	8.75	2.5	0.8
C	p_w/s	0.2	0.4	0.6

shape. A laser welding machine (fiber welding system) was used to weld the pieces together as demonstrated in Figure 2b. This Laser welding technology was chosen because it works well with thin-walled stainless steel and designed for reduces thermal distortion, surface scratches, and potential weld discontinuities that could affect the integrity of the sample during testing. Moreover, the welding wire, with a diameter of 1.5 mm, was made from the same stainless-steel grade as the base material. This ensures that the weld area is compatible with the metal and has the same mechanical properties throughout. Figure 2(c) illustrates the final samples.

Tensile test

Specimens were fabricated using 0.8 mm thick stainless steel (304) alloy sheets. Tensile tests were performed to ascertain the mechanical properties of the sheets. Tensile tests were conducted on specimens sized in accordance with ASTM E8/E8M [29], as seen in Figure 3. Table 3 presents the test results derived from the average of three specimens.

Buckling test

Three thin-walled cylindrical column specimens were tested under axial load to validate the numerical simulations. As shown in Figure 4b, the first specimen served as an unstiffened reference column (RC), while the second was stiffened with two I-shaped stiffeners, and the third was stiffened with two L-shaped stiffeners. The computer-controlled electronic universal testing machine type WDW-200E was used for the axial buckling test, as shown in Figure 4a. The axial load was applied at the upper end gradually with the rate of 1 mm/min. Steel cylinders were fitted to the ends of the column to prevent any localized distortion of the cross-section, as shown

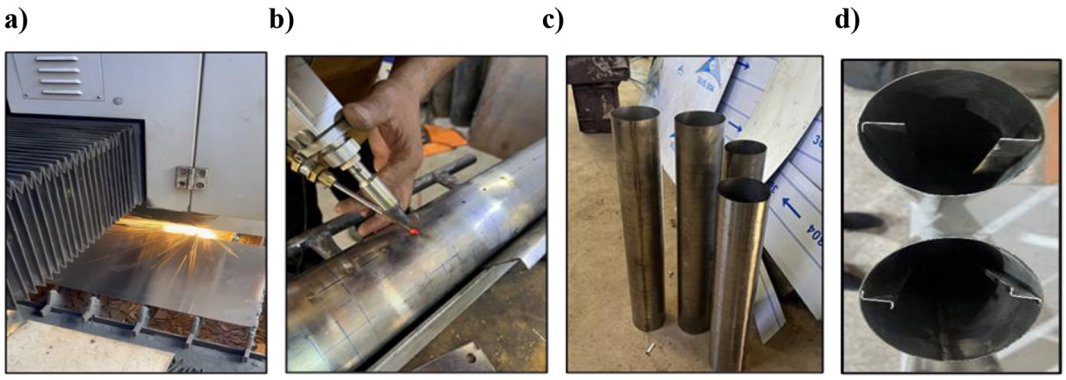

Figure 2. Manufacturing and welding process: (a) CNC fiber laser cutting machine; (b) fiber laser welding system; (c) specimen; (d) stiffened specimen

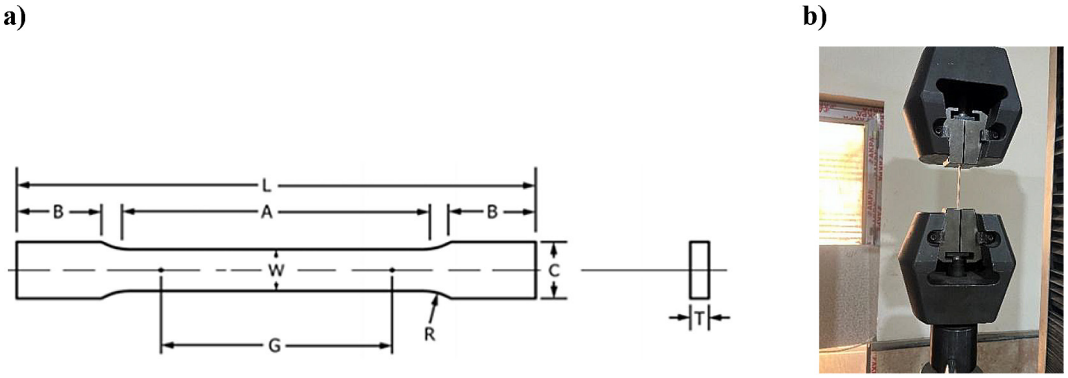

Figure 3. (a) Tensile test specimen dimensions according to ASTM E8/E8M All dimensions in mm, G: gage length 57, W: width 12.5, T: thickness 0.8, R: radius of fillet 12.5, A: length of reduced section 60, L: overall length 180, B: length of the grip section 50, C: width of the grip section 20; (b) tensile test specimens in the testing device

Table 3. Mechanical properties of SS304 stainless steel

Stainless steel (304)	Experimental measured
Young modulus, E (GPa)	195
Poisson's ratio, υ	0.29
Yield stress, σy (MPa)	270
Ultimate stress, σu (MPa)	510

in Figure 4c. The tests provided essential load–displacement data and buckling mode observations, enabling a direct and reliable correlation between the experimental results and the numerical predictions.

Finite element modelling

Thin-walled longitudinally stiffened columns were modeled and analyzed using Abaqus 2023 finite element software. All models were created according to the specimen dimensions. S4R elements were adopted for meshing due to their high accuracy in modeling thin-shell behavior and their capability to capture both local and global buckling modes. Each element has four nodes with six degrees of freedom (three translational and three rotational), allowing precise simulation of the thin column–stiffener interaction. The contact between the stiffeners and the cylindrical wall was defined as a tie constraint to represent the welded connection. Intermittent weld attachment was modeled using discrete circular tie regions, while weld flexibility and heat-affected zone softening were not explicitly considered, in line with assumptions commonly adopted in previous numerical studies. The potential influence of weld flexibility and residual stresses on local buckling initiation is therefore identified as a topic for future investigation. Axial compression was applied at the upper edge, while the bottom edge was fixed to prevent rigid-body motion. To replicate the experimental end cylinders used to avoid local cross-sectional distortion, the end nodes were coupled to reference points using kinematic constraints, enforcing uniform displacement and rotation consistent with the test setup. Initial geometric imperfections were incorporated in the nonlinear analyses by scaling the first linear buckling mode shape to an amplitude consistent with commonly adopted values in the literature. Although the absolute buckling loads are sensitive to imperfection magnitude, the comparative trends among different stiffener geometries and governing parameters were found to remain unchanged.

To trace the nonlinear post-buckling response, the Riks method was employed, which enables automatic control of the load–displacement path beyond the critical point and accurately captures the complete instability behavior. This procedure ensures convergence even when the structure experiences stiffness degradation after buckling initiation. The numerical framework was primarily intended to capture dominant main effects, while interaction effects among parameters were assessed qualitatively and found to be secondary within the investigated range. In Figure 5, only three representative simulation models are presented to illustrate the shape and position of the stiffeners within the thin-walled column. The results of all numerical models are reported and discussed in the Results section.

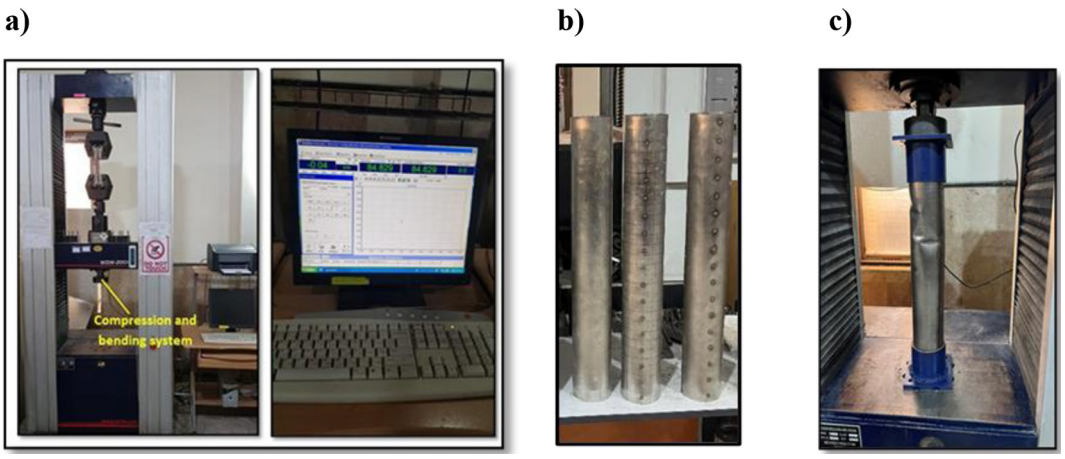

Figure 4. (a) WDW-200E universal testing machine; (b) specimen; (c) specimen in the testing device

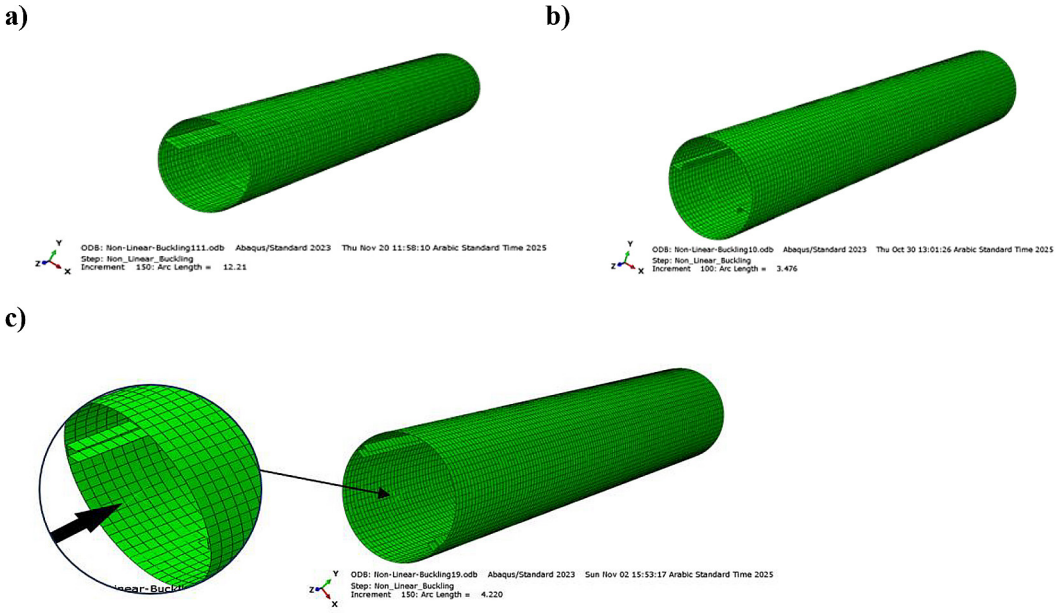

Figure 5. Columns geometry according to the experimental dimensions: (a) column with two I-shaped stiffeners; (b) column with two L-shaped stiffeners; (c) column with two U-shaped stiffeners

The numerical model as shown in Figure 6a, b, and c) explains the positions of the longitudinal stiffeners (I-, L-, and U-shaped) attached to the thin-walled stainless-steel cylinder using a discrete weld pattern that replicates the experimental configuration. The weld locations were defined along the stiffener centerline with a constant axial pitch of (p_w = 30 mm), measured from the loaded end to the fixed end, so that the spacing between successive attachment points matched the actual fabrication details. Each weld was idealized as a circular contact area with a nominal diameter of 5 mm, corresponding to the observed spot-weld footprint on the specimen surface. In the finite-element mesh, these regions were created by partitioning the shell of the thin column and the stiffener at the weld locations and applying tie constraints (surface-based or node-to-node) to enforce full compatibility of displacements between the stiffener and the column over the 5 mm circular zone.

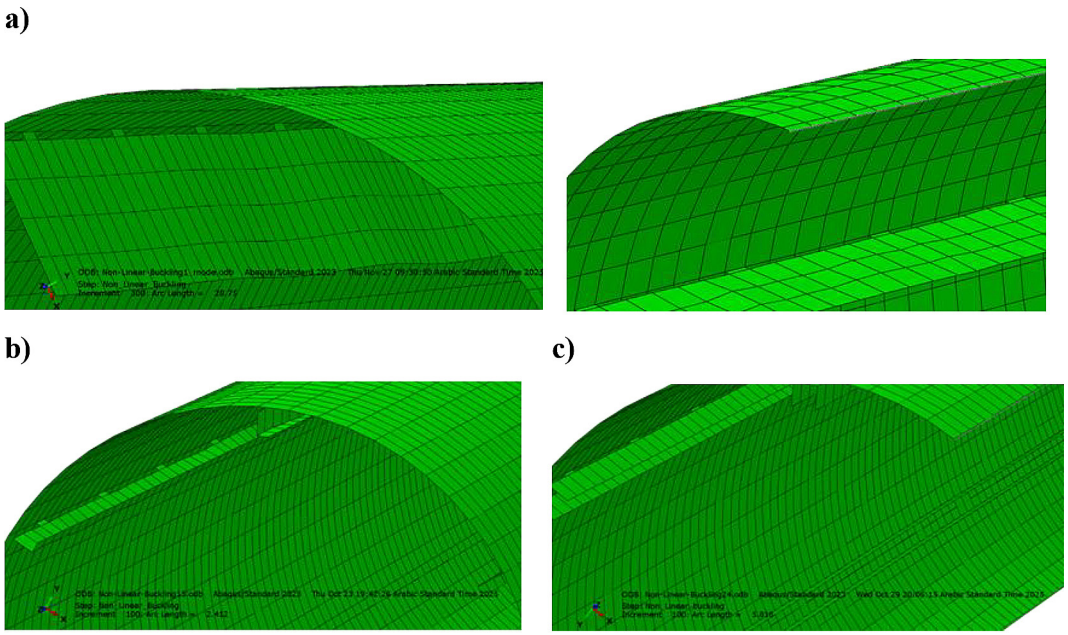

Figure 6. Stiffener geometry according to the weld locations dimensions: (a) I-shaped stiffener; (b) L-shaped stiffener; (c) U-shaped stiffener

This approach provides a realistic representation of local stiffness transfer from the stiffener to the cylindrical wall, which is critical for accurately predicting the onset and development of local buckling in the stiffened specimens. Weld material flexibility and heat-affected zone softening were not explicitly modeled; however, this idealization is consistent with common practice in shell buckling simulations and is considered sufficient for capturing the comparative buckling response among different stiffener geometries.

RESULTS AND DISCUSSION

Results of experimental tests

Experimental tests indicated that Thin-walled cylindrical columns without stiffeners (RC), illustrated in Figure 7c, and those with stiffeners, depicted in Figure 7a and 7b, were deformed under axial compression. The critical buckling load of the Thin-walled cylindrical columns increased with the addition of longitudinal stiffeners when subjected to axial compression, and the effect of the L-shaped stiffener on enhancing the critical buckling load is evident in this context. The observed deformation patterns and critical load values are important for validating the numerical simulation and ensuring the accuracy of the results. The experimental program was primarily designed to validate the numerical modeling strategy and boundary conditions rather than to exhaustively investigate all parametric configurations. Despite the limited number of tested specimens, the good agreement obtained between experimental and numerical results provides sufficient confidence in the finite element framework, which was subsequently extended to perform a comprehensive parametric study covering 27 numerical configurations**.** Table 4 lists the critical buckling load results for the three tested specimens.

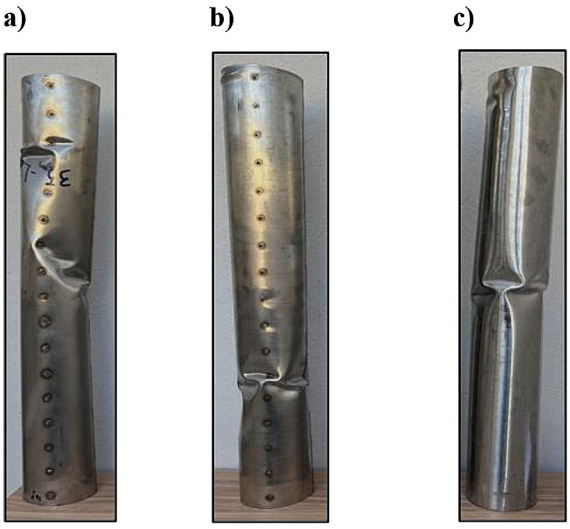

Figure 7. Buckling test results of columns: (a) I-shaped stiffened column; (b) L-shaped stiffened column; (c) unstiffened column

Results of finite elements analysis

The numerical analysis conducted using Abaqus demonstrated good agreement with the experimental results for the three tested specimens. Table 5 and Figure 8 present a comparison between the experimental and numerical critical buckling loads for both unstiffened and stiffened cylindrical columns, revealing a strong correlation between the two approaches. While the predicted critical buckling loads show close agreement, noticeable differences are observed in the post-buckling displacement response. These discrepancies are mainly attributed to the idealized representation of boundary conditions, the assumed geometric imperfection pattern and amplitude, and the absence of frictional effects and local compliance in the numerical model, which are inherently present in the experimental setup. It should be emphasized that the numerical framework was primarily developed to accurately predict the critical buckling load and associated buckling mode rather than to reproduce the full displacement evolution. Furthermore, Figure 9 confirms the similarity in the buckling modes observed experimentally and numerically, indicating that the failure of the tested specimens is governed by the interaction of local buckling and nonlinear structural response

Table 4. Experimental program results

Stiff. shape	Ns	b/ts	p_w/s	P_{EXP} (KN)
-	-	-	-	71.8
I	2	25	0.2	74.8
L	2	16.6	0.2	75.08

Table 5. Comparison of experimental and FEM critical buckling loads

Stiff. profile	Ns	b/ts	p_w/s	P_{EXP} (KN)	P_{FME} (KN)	P_{EXP}/P_{FEM}
-	-	-	-	71.8	66.1351	97.07%
I	2	25	0.2	74.8	75.32	99.3%
L	2	16.6	0.2	75.08	75.69	99.19%

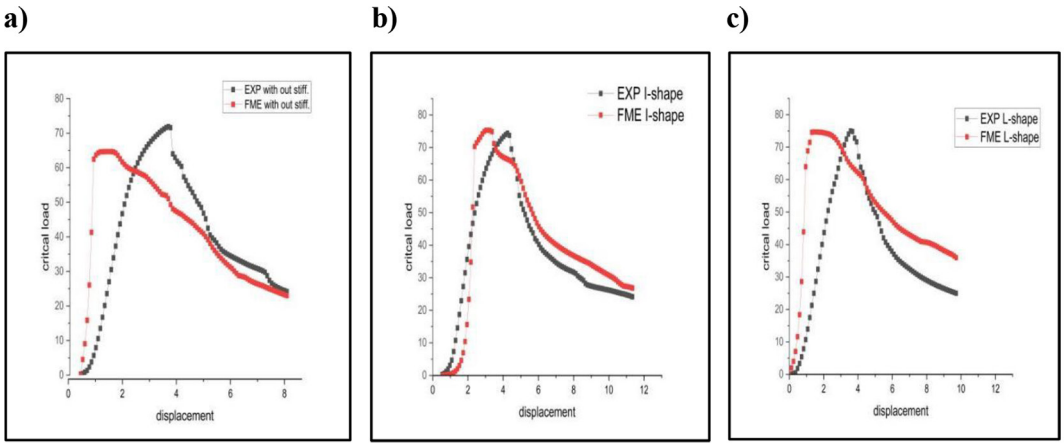

Figure 8. Comparison of experimental and FEM load–displacement curves for thin-walled cylindrical columns: (a) column without stiffeners; (b) column with two I-shaped stiffeners; (c) column with two L-shaped stiffeners

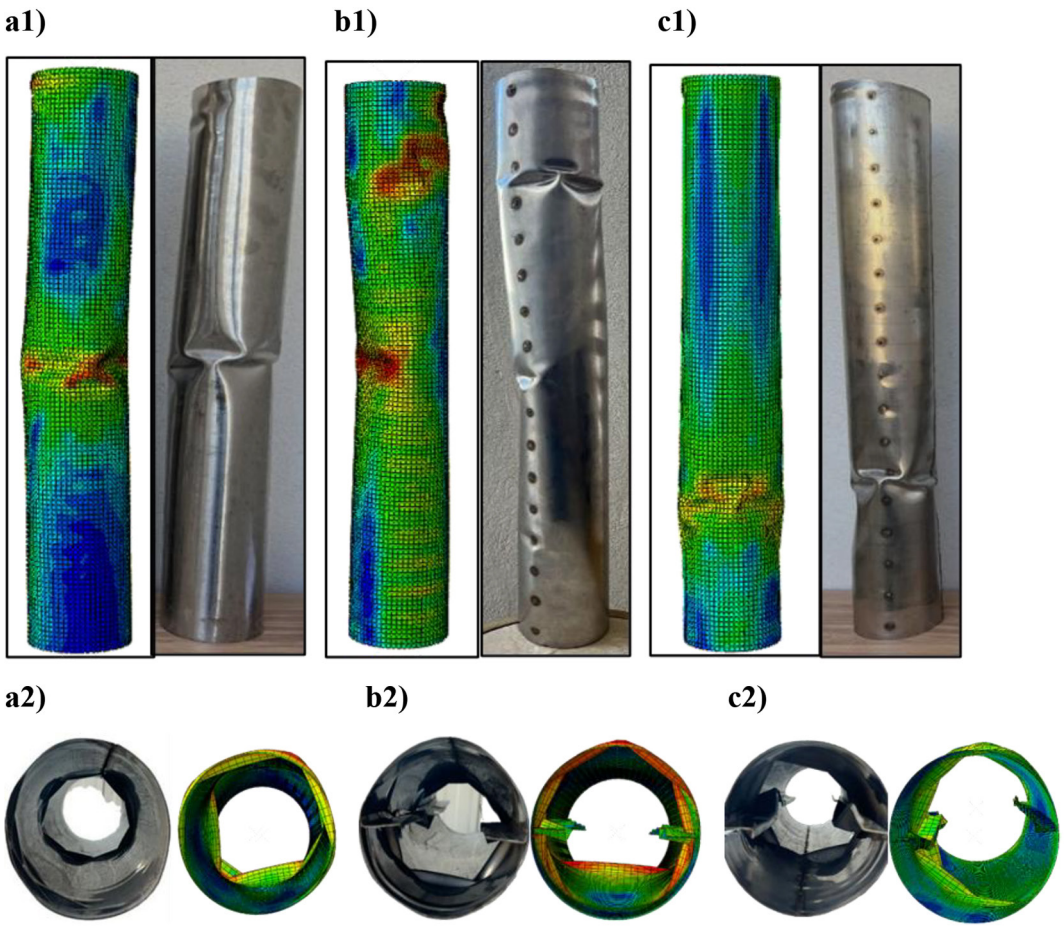

Figure 9. Comparison of buckling behaviors obtained from experimental tests and numerical simulations: a1–a2) column without stiffeners; b1–b2) column with two I-shaped stiffeners; c1–c2) column with two L-shaped stiffeners

under axial compression. Nonlinear buckling finite element studies were performed to determine the critical buckling load value. An orthogonal array including 27 combinations (L27) was developed. The critical buckling load value was computed for each combination. Table 6 presents the results of critical buckling from the simulation program.

The numerical program, consisting of 27 Abaqus models, systematically combined all stiffening variables three stiffener shapes (I, L, and U), three stiffener thicknesses (0.8, 1.6, and 2.4 mm), and three stiffener counts (2, 4, and 6) together with a weld space (p_w = 30 mm). This matrix enabled a comprehensive assessment of how stiffener shape, thickness, and circumferential distribution (p_w/s) influence the axial buckling resistance of thin-walled stainless-steel cylindrical columns. The results demonstrated a clear hierarchy of performance, where the U-shaped stiffeners produced the highest improvement, followed by the L-shaped and then the I-shaped configurations. Increasing the stiffener count significantly enhanced buckling strength, with all peak values occurring at (Ns = 6), as the circumferential stiffness and confinement improved and the effective panel width between stiffeners was minimized. Stiffener thickness also played a strong role, where moderate and large thicknesses (1.6 and 2.4 mm) increased local bending stiffness and strengthened the weld line, especially when combined with low (p_w/s) ratios that improved shear transfer and delayed the initiation of local buckling waves. Within this parameter space, the highest critical loads were recorded for U-shape, (Ns = 6, ts = 1.6, 91,574 kN), as shown in Figure 11c; L-shape, (Ns = 6, ts = 1.6, 89,567 N); L-shape, (Ns = 6, ts = 2.4, 89,567 N), as shown in Figure 11b; and I-shape, (Ns = 6, ts = 2.4, 86,621 N), as shown in Figure 11a, confirming

Table 6. Orthogonal array with the critical load

Test No.	Thickness of stiffener mm	High stiffeners (b) mm	shape	Ns	p_w/s	b/ts	Critical load (comp.) N
1	0.8	20	I	2	0.2	25	75323
2	0.8	20	I	4	0.4	25	73567
3	0.8	20	I	6	0.6	25	74349
4	1.6	10	I	2	0.2	6.25	72396
5	1.6	10	I	4	0.4	6.25	76186
6	1.6	10	I	6	0.6	6.25	81521
7	2.4	7	I	2	0.2	2.9	73539
8	2.4	7	I	4	0.4	2.9	80352
9	2.4	7	I	6	0.6	2.9	86622
10	0.8	13.5	L	2	0.2	16.6	74692
11	0.8	13.5	L	4	0.4	16.6	79023
12	0.8	13.5	L	6	0.6	16.6	89084
13	1.6	7	L	2	0.2	4.3	70178
14	1.6	7	L	4	0.4	4.3	79023
15	1.6	7	L	6	0.6	4.3	89567
16	2.4	5	L	2	0.2	2	72671
17	2.4	5	L	4	0.4	2	78118
18	2.4	5	L	6	0.6	2	89567
19	0.8	7	U	2	0.2	8.75	74320
20	0.8	7	U	4	0.4	8.75	82101
21	0.8	7	U	6	0.6	8.75	89084
22	1.6	3.5	U	2	0.2	2.2	72840
23	1.6	3.5	U	4	0.4	2.2	82212
24	1.6	3.5	U	6	0.6	2.2	91574
25	2.4	2	U	2	0.2	0.8	68337
26	2.4	2	U	4	0.4	0.8	71908
27	2.4	2	U	6	0.6	0.8	87772

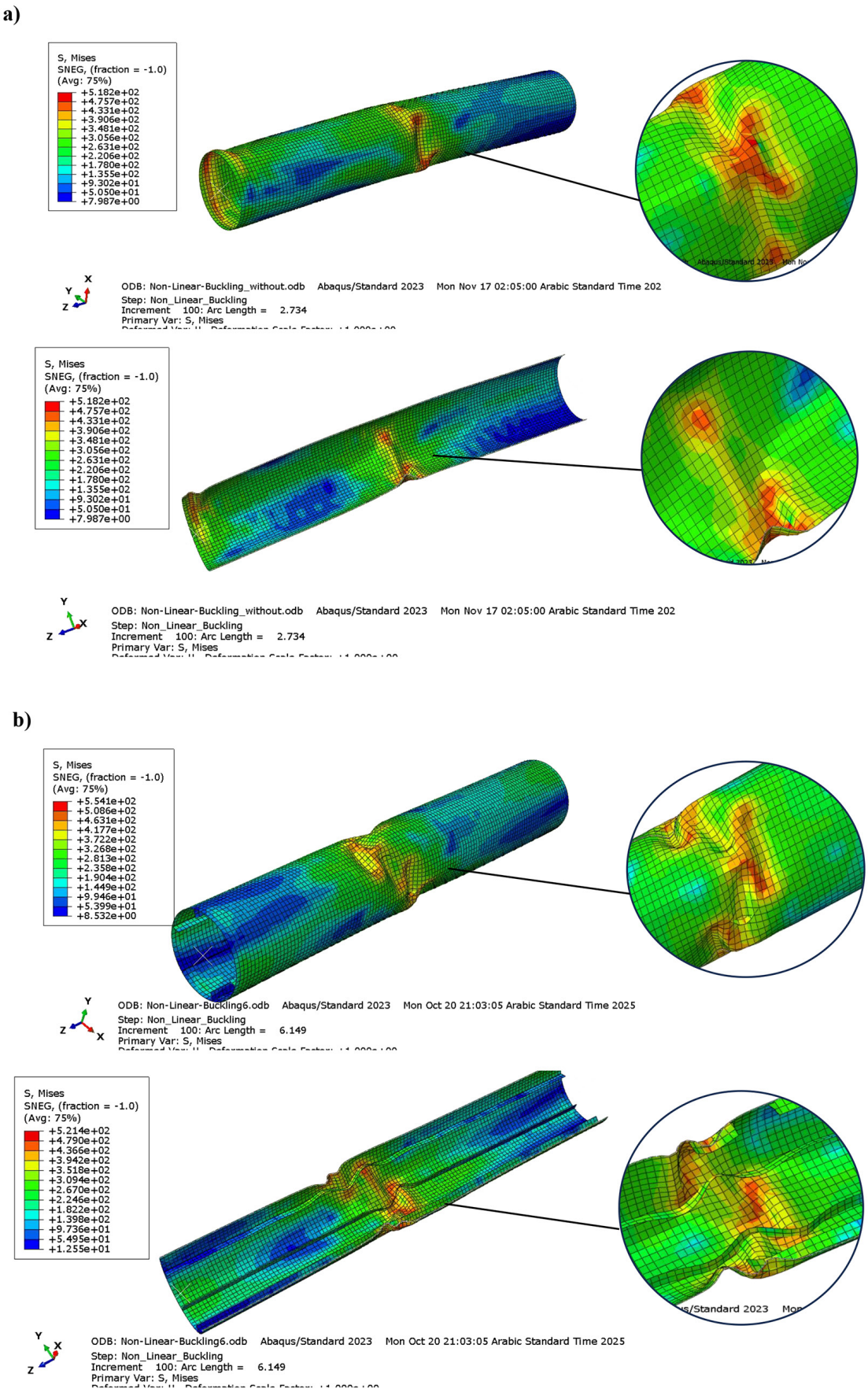

Figure 10. The results for the critical buckling load obtained from simulation analysis: (a) without stiffener; (b) I-shape stiffener; (c) L-shape stiffener; (d) U-shape stiffener

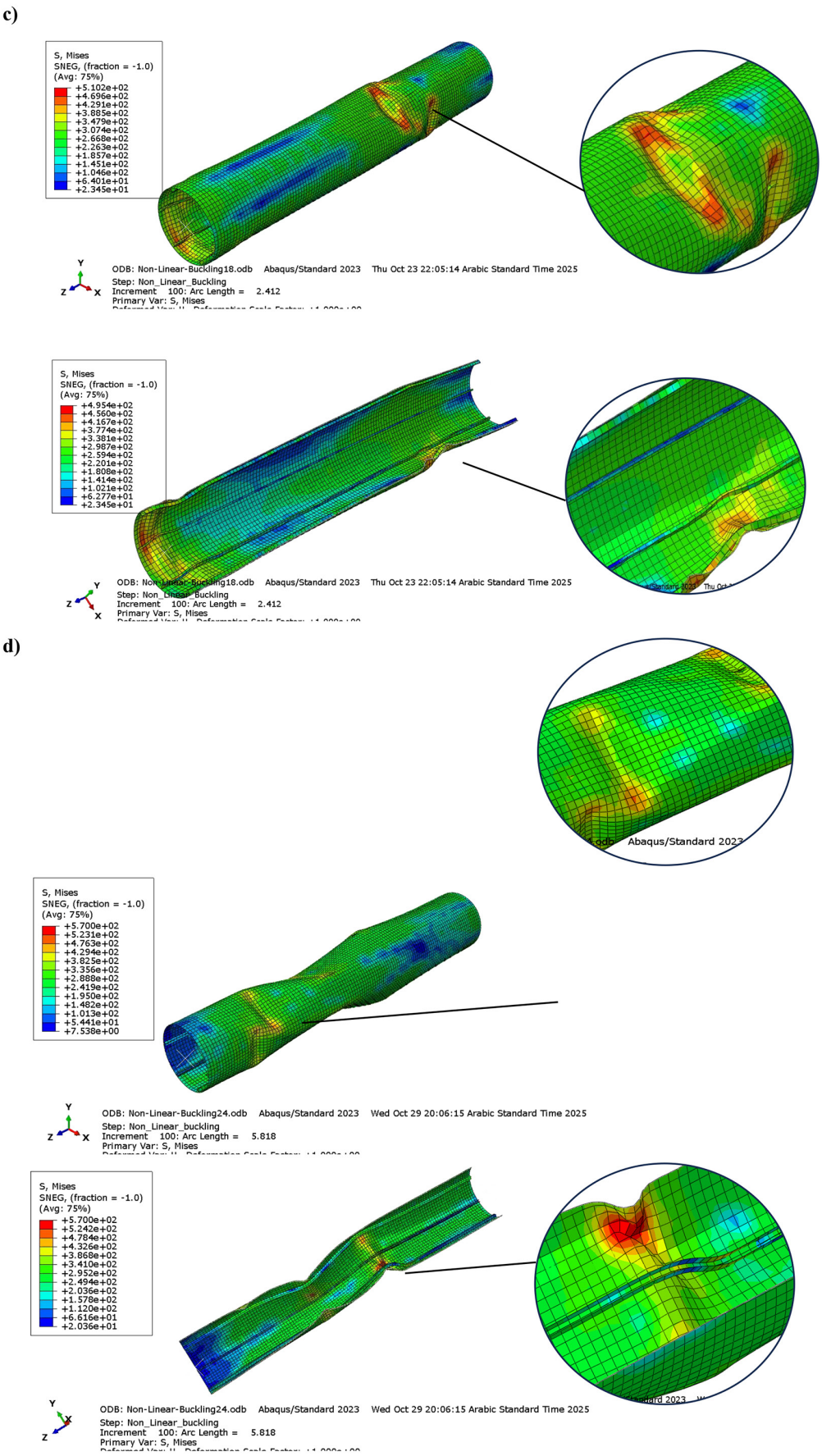

Figure 10. The results for the critical buckling load obtained from simulation analysis: (a) without stiffener; (b) I-shape stiffener; (c) L-shape stiffener; (d) U-shape stiffener

the superior stabilizing effect of using six stiffeners with low spacing ratios.The exceptional performance of the U-shape configuration is attributed to its semi-closed geometry, dual weld legs, enhanced circumferential restraint, and optimal balance between stiffener stiffness and shell engagement, which collectively minimized ovalization. Overall, the results highlight that stiffener geometry is the dominant variable controlling buckling behavior and that the combination of a U-profile, six stiffeners, and moderate thickness provides the most effective enhancement of axial buckling resistance. Figure 10 shows the numerical results for the critical buckling load obtained from simulation analysis. Figures of the specimens with the highest critical buckling load value were chosen for presentation in this paper. Overall, when the mass of stiffener remains constant, the stiffener geometry significantly influences the buckling resistance of the thin-walled column specimen.

Figure 11 illustrates the load–displacement responses of unstiffened and stiffened thin-walled SS304 cylindrical columns incorporating I-, L-, and U-shaped longitudinal stiffeners. In all cases, the initial linear segments of the curves correspond to elastic behavior, followed by nonlinear softening associated with the initiation of local buckling. Relative to the unstiffened reference column, all stiffened configurations exhibit a pronounced enhancement in critical buckling strength. Based on the maximum recorded loads, the I-shaped stiffener achieved an increase in critical load of approximately 20.6%, while higher improvements in the range of 24.7–27.5% were obtained for the L-shaped and U-shaped stiffeners, respectively. Furthermore, when compared at peak capacity, the L-shaped and U-shaped configurations exceeded the I-shaped stiffener by approximately 3.4–5.7%, respectively, whereas the difference between the L-shaped and U-shaped stiffeners remained relatively small approximately 2.2%.

Beyond the peak load, the post-buckling displacement response reveals clear differences

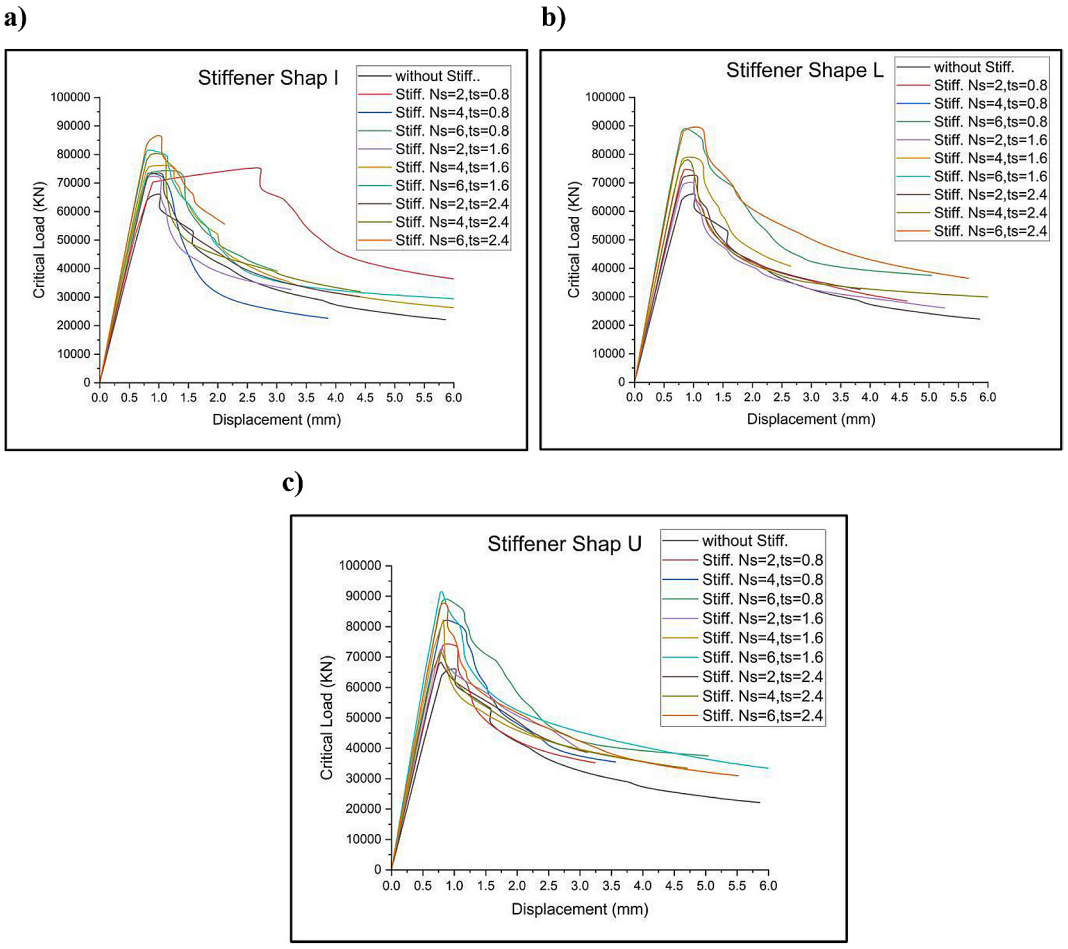

Figure 11. Critical buckling load–displacement diagrams for all stiffener families: (a) I-shaped stiffeners; (b) L-shaped stiffeners; (c) U-shaped stiffeners

among the stiffener geometries, reflecting variations in stiffness redistribution, local buckling development, and shear-lag sensitivity. Columns stiffened with I-shaped profiles exhibit a pronounced post-peak load reduction accompanied by limited deformation capacity, particularly at lower stiffener densities, owing to the open-section geometry, shear-lag effects, and the rapid development of local buckling in the shell panels between stiffener weld lines. The L-shaped stiffener demonstrates improved post-peak behavior with a more gradual load reduction and increased displacement capacity, reflecting enhanced local restraint of the thin-wall; however, the asymmetric stiffness distribution still promotes localized deformations in less-supported regions. In contrast, the U-shaped stiffener provides the most stable post-buckling response, sustaining higher load levels over larger displacements. This superior behavior is attributed to its semi-closed geometry, which enhances circumferential confinement, improves load transfer between the stiffener and thin column, and effectively suppresses the growth of local buckling waves. The post-buckling performance is therefore assessed qualitatively based on the shape of the load–displacement curves; a quantitative evaluation of ductility or energy absorption capacity (e.g., area under the curve) is recommended as a valuable extension for future work.

Overall, increasing the number of stiffeners significantly improves both peak load and post-buckling displacement capacity for all geometries, whereas variations in stiffener thickness achieve a comparatively secondary role, confirming that circumferential stiffener distribution governs both strength and stability after buckling.

Taguchi and ANOVA results

The Taguchi method was employed to systematically assess the influence of the governing design parameters on the buckling performance of longitudinally stiffened thin-walled cylindrical columns. An orthogonal array was adopted to accommodate three factors at three levels while ensuring a balanced and statistically efficient design, as summarized in Table 7. The selected control parameters included the stiffener geometry (I-, L-, and U-shaped), the number of stiffeners (Ns), and the stiffener thickness (ts). For each of the 27 numerical runs prescribed by the orthogonal array, the critical compressive buckling load was taken as the response variable (Y1), and the corresponding signal-to-noise (S/N) ratio was evaluated using the "larger-is-better" criterion. It should be noted that the circumferential spacing ratio (p_w/s) was not treated as an independent parameter in the Taguchi matrix. This decision was made because (p_w/s) is directly governed by the number of stiffeners (Ns) through geometric compatibility and therefore represents the same physical effect. Including both parameters in the Taguchi design would result in redundancy and potential overrepresentation of the circumferential stiffness effect. Consequently, the influence of (p_w/s) is inherently captured through variations in Ns. Similarly, the stiffener slenderness ratio (b/ts) is effectively governed by the stiffener thickness (ts) within the present design framework. In order to maintain a constant stiffener mass across all configurations, the stiffener width (b) was adjusted accordingly with changes in (ts), and its value varied depending on the selected stiffener geometry. This equal-mass constraint ensures a fair comparison among different stiffener shapes and thickness levels by eliminating mass as a confounding parameter. Consequently, the investigated levels of (b/ts) correspond directly to (ts = 0.8, 1.6, and 2.4 mm), while implicitly accounting for the geometry-dependent variation of (b). In this context, the effect attributed to (b/ts) in the Taguchi analysis primarily reflects the influence of thickness-controlled, equal-mass stiffener configurations on the buckling behavior, rather than the isolated effect of thickness alone.

The results summarized in Tables 8–9 and quantitatively confirmed by the Taguchi response table for the signal-to-noise ratio (Table 7) demonstrate that the number of stiffeners (Ns) is the dominant parameter governing the buckling resistance of longitudinally stiffened Thin-walled cylindrical columns. This is evidenced by the highest Delta value ($\Delta = 1.50$) and the consistent increase in both critical buckling load and S/N ratio when Ns increases from Level 1 to Level 3, with the most robust performance observed at (Ns = 6). This behavior reflects the decisive role of circumferential stiffness redistribution and the reduction of unstiffened thin wall width in buckling resistance. Stiffener geometry ranks second in significance ($\Delta = 0.33$), where L- and U-shaped stiffeners outperform the I-shaped configuration due to their enhanced torsional rigidity and more effective thin wall stiffener interaction under equal-mass conditions. In contrast, stiffener

Table 7. Orthogonal array and S/N

Run No.	A: Shape of Stiffener	B: Number of Stiffeners (Ns)	C: b/ts	Response Y1 (N)	S/N (Larger)
1	I	2	0.8	75322.9	97.5385
2	I	2	1.6	72396.4	97.1943
3	I	2	2.4	73539.0	97.3304
4	I	4	0.8	73566.8	97.3336
5	I	4	1.6	76185.9	97.6375
6	I	4	2.4	80351.9	98.0999
7	I	6	0.8	74349.4	97.4255
8	I	6	1.6	81521.1	98.2254
9	I	6	2.4	86621.5	98.7525
10	L	2	0.8	74692.1	97.4655
11	L	2	1.6	70177.8	96.9240
12	L	2	2.4	72671.0	97.2272
13	L	4	0.8	79023.4	97.9551
14	L	4	1.6	79023.4	97.9551
15	L	4	2.4	78118.4	97.8551
16	L	6	0.8	89084.1	98.9960
17	L	6	1.6	89567.1	99.0430
18	L	6	2.4	89567.1	99.0430
19	U	2	0.8	74319.8	97.4221
20	U	2	1.6	72840.4	97.2474
21	U	2	2.4	68336.5	96.6931
22	U	4	0.8	82101.1	98.2870
23	U	4	1.6	82212.2	98.2987
24	U	4	2.4	71907.7	97.1355
25	U	6	0.8	89084.1	98.9960
26	U	6	1.6	91574.0	99.2354
27	U	6	2.4	87771.7	98.8671

thickness (ts) exhibits the weakest influence (Δ = 0.08), indicating that its effect is secondary within the investigated range. An intermediate thickness of (ts = 1.6 mm) provides an optimal balance between stiffness enhancement and stress compatibility, particularly at higher Ns levels, where the maximum S/N ratio of approximately 99.24 dB is achieved. The closely spaced response values observed in several Taguchi runs are attributed to the discrete nature of the orthogonal array levels rather than numerical inconsistency. Overall, the ranking Ns > Shape > ts is fully consistent with the observed buckling trends and provides a statistically supported basis for identifying the optimal stiffening configuration (Figure 12).

Overall, the Taguchi and ANOVA analyses confirm that the number of stiffeners is the dominant parameter controlling buckling resistance, followed by stiffener geometry, while the influence of stiffener thickness (or equivalently b/ts) is of secondary importance within the investigated parameter space.

Discussion of b/ts, stiffener shape, and thickness effects

The influence of the stiffener height-to-thickness ratio (b/ts) on the axial critical load demonstrates a strong dependence on stiffener geometry, even though all stiffener configurations were designed with equal mass, making the comparison entirely shape-driven. As shown in Figure 13c, the U-shaped stiffener consistently provides the highest critical load. The cross-sections with semi-closed geometry deliver superior torsional rigidity, enhanced warping restraint, and more efficient distribution of axial stresses along the thin-walls an effect widely documented in

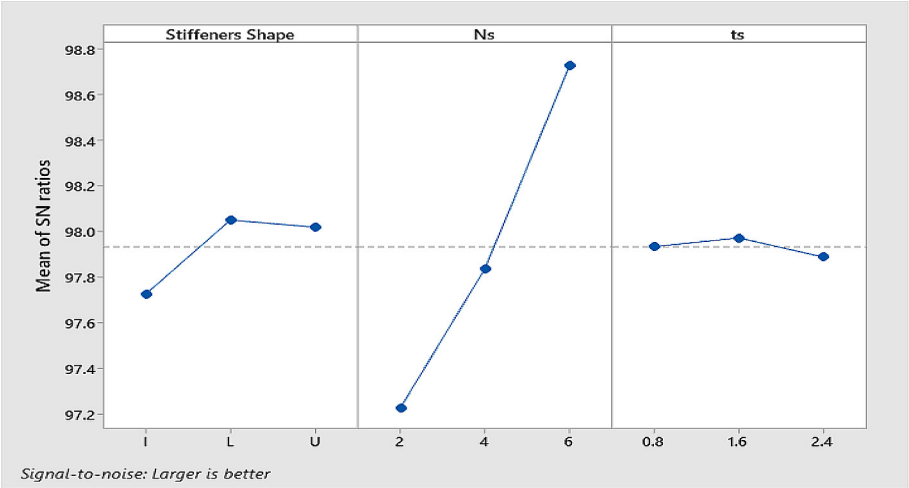

Figure 12. Main effect plot of S/N ratios

Table 8. Combined Taguchi mean S/N analysis including the shape factor

Symbol	Rank	Factor	Level 1	Level 2	Level 3	Delta	Influence
B	1	Ns	97.23	97.84	98.73	1.5	Strongest
A	2	Shape	97.73	98.05	98.02	0.33	Medium
C	3	ts	97.94	97.97	97.89	0.08	Weak

Table 9. The results of ANOVA for the combined stiffener parameters

Factor	Sum Sq.	DOF	Mean Sq	F-value	p-value
Ns	10.304	2	5.152	26.86	0
Stiffeners Shape	0.5791	2	0.28955	1.51	0.245
ts	0.032	2	0.01598	0.08	0.92
Error	3.8366	20	0.19183	-	-
Total	14.7517	26	-	-	-

studies examining the stability of stiffened cylindrical columns [7,8,30]. In contrast, the open-web I-section, despite having identical mass, exhibits lower rotational stiffness and greater sensitivity to shear-lag and local buckling. Such vulnerabilities of open stiffener sections have been reported in prior investigations on welded and thin-walled members, where shear-lag and premature local instability significantly reduced the attainable buckling strength [10,31,32]. These insights explain why increasing (b/ts) in the I-shape does not generate proportional improvements in global stability, particularly at larger stiffener numbers. Although the present interpretation is based on qualitative sectional behavior, a detailed quantitative comparison of bending and torsional stiffness properties is suggested as a valuable extension for future work to further substantiate the observed performance differences among stiffener geometries.

Conversely, both the L- and U-shaped stiffeners benefit substantially from increases in (b/ts), especially for (Ns = 4 and 6), where the additional stiffener height enhances rigidity and confinement, promoting more effective composite action between the stiffener and the cylindrical wall. Similar mechanisms have been identified in stiffened panels and cylindrical columns, where increased confinement and bending stiffness delayed local buckling and raised global collapse loads [33–35]. The ability of the L and U shapes to redistribute compressive stresses more uniformly along the shell helps postpone the formation of localized buckling waves and yields a noticeable improvement in critical load. The effect of stiffener thickness (ts) further supports this interpretation.

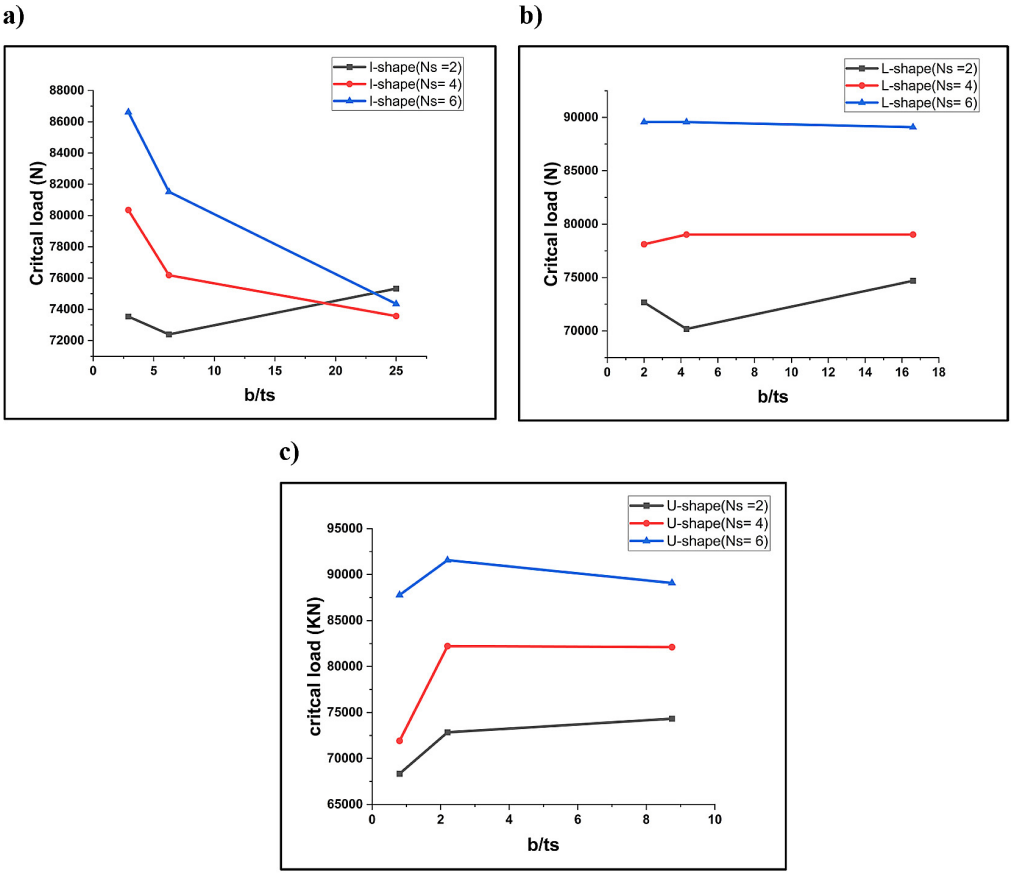

Figure 13. Effect of the stiffener height-to-thickness ratio (b/ts) on the axial critical load: (a) I-shaped stiffeners; (b) L-shaped stiffeners; (c) U-shaped stiffeners

Discussion of the influence of circumferential spacing ratio (p_w/s) on the critical load

The effect of the circumferential spacing ratio (p_w/s) on the axial critical load shows a clear and consistent trend across all stiffener configurations, as illustrated in Figures 14. Increasing (p_w/s) corresponding to larger weld spacing relative to stiffener spacing produces a substantial enhancement in the load-carrying capacity of the stiffened column. For the I-shaped stiffeners, the critical load increases steadily at all levels of Ns, with the improvement becoming most pronounced when (Ns = 6). This behavior suggests that wider circumferential spacing reduces the mechanical interaction between adjacent stiffeners, promoting a more uniform distribution of membrane stresses, lowering localized restraint, and delaying the onset of circumferential local buckling. Similar stress redistribution mechanisms and spacing effects have been documented in studies of stiffened cylindrical shells and conical shells under axial compression [30,8,36], while analyses of imperfection-sensitive shells indicate that excessive stiffener crowding can trigger early instability [3,35]. A similar positive trend is observed for both the L- and U-shaped stiffeners, where increasing (p_w/s) consistently leads to higher critical loads for all stiffener thicknesses. However, the magnitude of improvement remains shape-dependent. The L-shaped specimens exhibit moderate gains in capacity with increasing spacing, consistent with their partially closed geometry that provides reasonable torsional restraint but still allows localized stress intensification when stiffeners are closely positioned. In contrast, the U-shaped stiffener configuration shows the strongest enhancement at higher (p_w/s), particularly when (ts = 1.6 mm), illustrating the ability of semi-closed profiles to redistribute circumferential stresses effectively and suppress instability mechanisms. Comparable behavior has been noted in stiffened panels and cylindrical columns, where semi-closed or closed stiffeners reduce mutual interference and enhance global stability under axial loading [33–35]. A key observation is that the response to (p_w/s) is significantly influenced by stiffener thickness.

For both the L- and U-shaped stiffeners, the 1.6 mm thickness consistently yields the highest critical loads across all spacing ratios, confirming that this thickness represents an optimal balance of stiffness for promoting composite action with the thin column. Conversely, the thickest stiffeners (ts = 2.4 mm) exhibit reduced sensitivity to increases in (p_w/s) due to stiffness mismatch, which promotes localized shell instability rather than global strengthening.Similar findings have been reported in studies where overly stiff stiffeners introduced sharp stress gradients, concentrating stresses at weld interfaces and reducing buckling efficiency [9,37,38]. Overall, the results demonstrate that increasing circumferential spacing (higher p_w/s) enhances structural efficiency by minimizing stiffener–stiffener interaction, suppressing local instability, and enabling more uniform circumferential stress distribution along the cylindrical wall. The magnitude of improvement strongly depends on stiffener geometry, with the U-shaped configuration providing the most substantial gains under equal-mass conditions a finding consistent with prior work on the superior stability performance of semi-closed stiffening profiles [7,8,30].

Effect of stiffeners number

The critical load increases consistently with the number of stiffeners (Ns) for all stiffener shapes, as shown in Figures 15. Increasing Ns reduces the circumferential unsupported length of the thin-walled cylindrical column and enhances its global stiffness, thereby delaying both local and overall buckling. This trend is well aligned with classical and modern studies on stiffened thin- wall cylindrical columns, which demonstrate that increasing the number of stiffening elements significantly improves structural stability by redistributing membrane stresses and suppressing localized deformation modes [30,35,36]. The magnitude of improvement, however, is strongly dependent on stiffener geometry. The U-shaped stiffener shows the largest gains with increasing Ns due to its semi-closed form, which

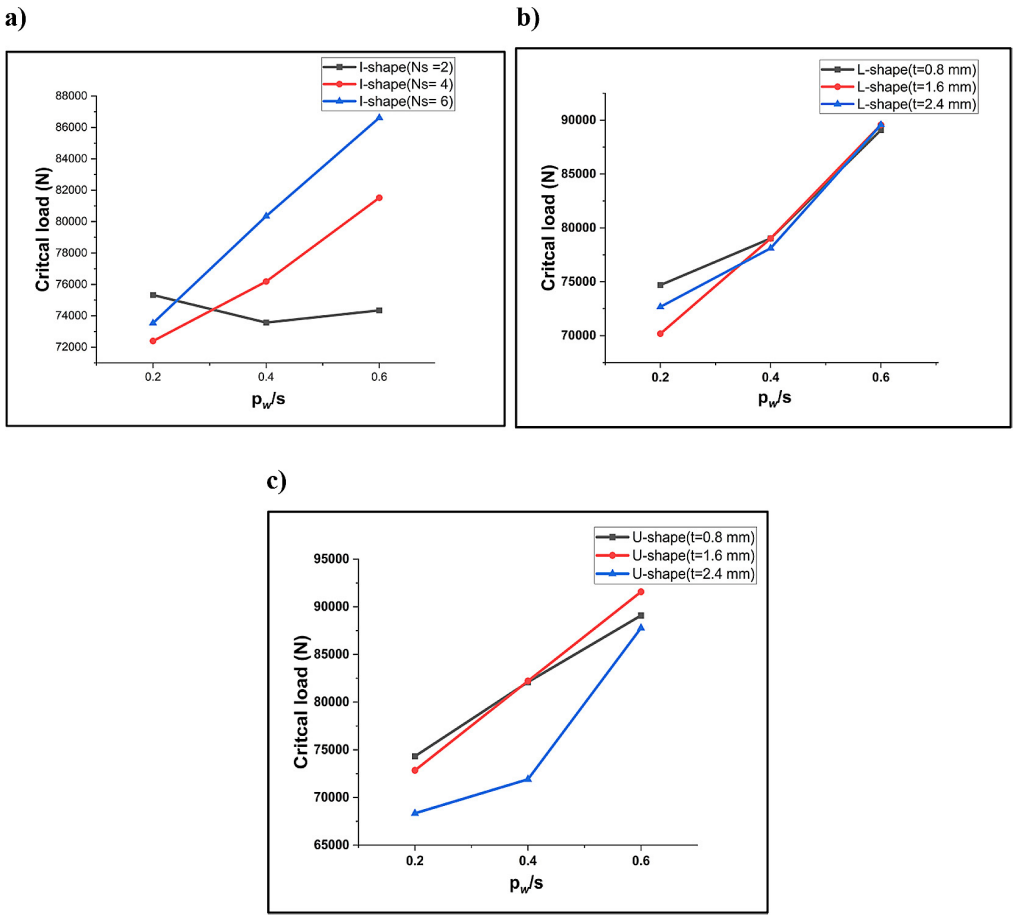

Figure 14. Effect of the circumferential spacing ratio (p_w/s) on the axial critical load: (a) I-shaped stiffeners; (b) L-shaped stiffeners; (c) U-shaped stiffeners

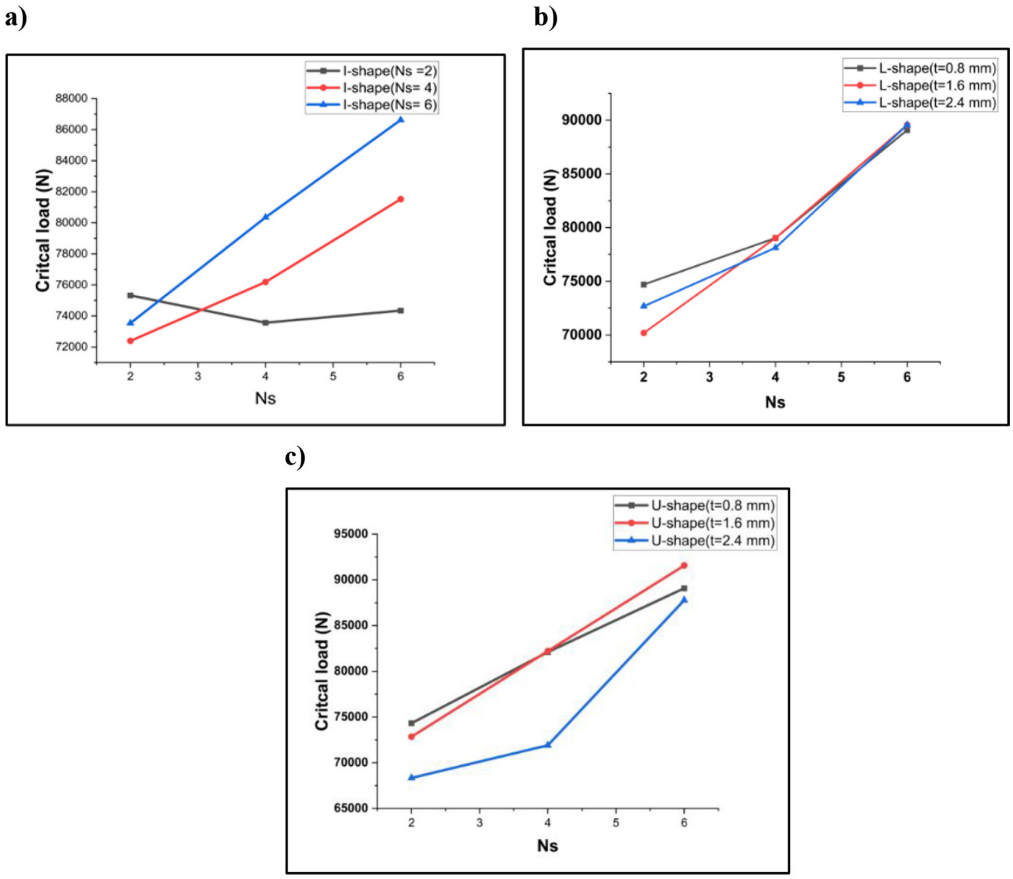

Figure 15. Effect of the number of stiffeners (Ns) on the axial critical load for all stiffener shapes: (a) I-shaped stiffeners; (b) L-shaped stiffeners; (c) U-shaped stiffeners

provides higher torsional rigidity and more effective confinement of the shell wall behaviors previously highlighted in investigations of stiffened plates and semi-closed stiffener systems [8,33]. The L-shaped stiffener exhibits moderate but consistent improvements, with its partially closed geometry offering enhanced bending stiffness but remaining susceptible to localized stress intensification at lower Ns levels. In contrast, the I-shaped stiffener, despite equal mass, shows the least improvement because its open-web configuration is more vulnerable to shear-lag effects and local flange buckling. This observation aligns with prior findings on the inferior torsional rigidity and instability sensitivity of open-section stiffeners under axial compression [10,31,32].

CONCLUSIONS

This work studied the effects of Three different longitudinal stiffener geometries (I-, L-, and U-shaped) are systematically compared under equal mass conditions on the buckling behavior of thin-walled SS304 cylindrical columns. By integrating nonlinear numerical simulations with experimental observations. Systematically quantified stiffening parameters to achieve best critical load value. The Taguchi and ANOVA methods were applied to analyze the outcomes of the finite element to specify the effect of the parameters and their combinations. The results demonstrate that the stiffener circumferential spacing ratio ($p_w/s = 2.2$) and the number of stiffeners (Ns = 6) have the strongest impact on buckling resistance. Furthermore, when comparing the longitudinal stiffener geometries, the L-shaped and U-shaped stiffeners exceeded the I-shaped configuration. By increasing the critical load value approximately 3.4% and 5.7%, respectively, whereas the difference between the L-shaped and U-shaped stiffeners remained relatively small (about 2.2%). These findings indicate that the U-shaped stiffener provides the highest buckling resistance and overall structural efficiency, while the L-shaped stiffener represents a practical and effective alternative when lower manufacturing cost is prioritized. The I-shaped stiffener remains a viable

design option; however, it exhibits comparatively lower stability performance and higher sensitivity to shear-lag effects and local buckling. Future studies may extend the present investigation by applying the same stiffener configurations under different loading orientations, such as lateral, torsional, or combined axial-bending actions, to evaluate directional sensitivity in buckling resistance and enhance applicability to realistic structural conditions.

REFERENCES

1. Buckling of thin-walled cylinders. SP-8007. Washington (DC): NASA; 1968.
2. Timoshenko SP, Gere JM, Prager W. Theory of elastic stability, second edition. J Appl Mech. 1962; 29:220–221.
3. Singer J, Arbocz J, Weller T. Buckling experiments: experimental methods in buckling of thin-walled structures: shells, built-up structures, composites and additional topics. Hoboken (NJ): John Wiley & Sons; 2008.
4. Schneider W, Brede A. Consistent equivalent geometric imperfections for the numerical buckling strength verification of cylindrical shells under uniform external pressure. Thin-Walled Struct. 2005;43(2):175–188. https://doi.org/10.1016/j.tws.2004.08.005
5. Teng JG. Buckling of thin shells: recent advances and trends. Appl Mech Rev. 1996;49(4):263–274. https://doi.org/10.1115/1.3101926
6. Buermann P, Rolfes R, Teßmer J, Schagerl M. A semi-analytical model for local post-buckling analysis of stringer- and frame-stiffened cylindrical panels. Thin-Walled Struct. 2006;44:102–114. https://doi.org/10.1016/j.tws.2006.01.002
7. Lee KC, Yoo C. Longitudinal stiffeners in concrete-filled tubes. J Struct Eng. 2012;138:753–758. https://doi.org/10.1061/(ASCE)ST.1943-541X.0000523
8. Shiomitsu D, Yanagihara D. Elastic local shell and stiffener-tripping buckling strength of ring-stiffened cylindrical shells under external pressure. Thin-Walled Struct. 2020;148:106622. https://doi.org/10.1016/j.tws.2019.106622
9. Bardi FC, Kyriakides S. Plastic buckling of circular tubes under axial compression—part I: experiments. Int J Mech Sci. 2006;48(8):830–841. https://doi.org/10.1016/j.ijmecsci.2006.04.007
10. Abedin MZ, Maleki S, Kiani N, Shahrokhinasab E. Shear lag effects in angles welded at both legs. Adv Civ Eng. 2019;2019: Article ID 7313632. https://doi.org/10.1155/2019/7313632
11. Hulka I, Ungureanu V, Both I, Petzek E, Radu B. Influence of resistance spot welding parameters on cold-formed steel properties and failure modes. Civ Eng J. 2025;11(6):2170–2188.
12. Yenugula V, Gunda J, Pinninti RR, Markandeya R. Non-linear buckling and post-buckling analysis of cylindrical shells subjected to axial compressive loads: a study on imperfection sensitivity. Nonlinear Eng. 2013;2:1–15.
13. Nguyen PC, Tran TT, Nguyen HP, Tran TD. Nonlinear inelastic local buckling behavior of steel columns subjected to axial compression. Civ Eng J. 2025;11(9):3916–3933.
14. Kifumbi FM, Ngoma GD, Erchiqui F, Tshibangu TM. Experimental and numerical modeling of a cross-flow turbine runner made of HDPE: experimental and numerical approach. HighTech Innov J. 2025;6(4):1104–1122.
15. Mushattat SM, Al-Alkawi HJM, Raja AH. Electromechanical design and manufacturing of dynamic buckling test rig under various temperature conditions. Eng Technol J. 2022;40(1):233–240.
16. Al-Khafaji HMH. Best level of parameters for a critical buckling load for circular thin-walled structure subjected to bending. Al-Khwarizmi Eng J. 2019;13(4):12–21.
17. Al-Khafaji HMH. Optimisation of the lateral buckling strength of corrugated composite material plate by neural networks method. IOP Conf Ser Mater Sci Eng. 2020;788:012037. https://doi.org/10.1088/1757-899X/788/1/012037
18. Al-Khafaji HMH, Swadi NN, Hadi AS. Optimizing the modified Whitworth quick return mechanism using Taguchi and ANOVA methods. Int Rev Mech Eng. 2022;16(3):145–154.
19. Galambos TV. Guide to stability design criteria for metal structures. 5th ed. New York: John Wiley & Sons; 1998.
20. Pinninti RR, et al. Nonlinear buckling and post-buckling analysis of imperfect cylindrical shells subjected to axial compressive load. J Struct Eng. 2015;42:78–85.
21. Deshpande S. Buckling and post buckling of structural components [master's thesis]. Arlington (TX): University of Texas at Arlington; 2010.
22. Lin JC, Lee K. Optimization of bending process parameters for seamless tubes using Taguchi method and finite element method. Adv Mater Sci Eng. 2015;2015:Article ID 148392. https://doi.org/10.1155/2015/148392
23. Al-Khafaji MMH, Al-Khafaji HMH. Taguchi method for analysing sliding surface parameters of an adaptive terminal sliding mode controller for an articulated robot. Int Rev Aerosp Eng. 2023;16(4):193–201.

24. Phadke MS. Quality engineering using robust design. New Jersey: PTR Prentice Hall; 1989.
25. Miller RG. Beyond ANOVA: basics of applied statistics. Canada: John Wiley & Sons; 1986.
26. Eurocode 3: design of steel structures—part 1–6: strength and stability of shell structures. Brussels: CEN; 2025.
27. Schulz E, et al. Short-pulse resistance spot welding of aluminum alloy 6016-T4 – part 1. Weld J. 2021;100:41–51.
28. Duspara M, et al. Optimization of nitrogen use efficiency in cutting of austenitic stainless steel by a fiber laser. FME Trans. 2022;50:745–751.
29. ASTM International. ASTM E8/E8M-21: standard test methods for tension testing of metallic materials. West Conshohocken (PA): ASTM; 2021.
30. Spagnoli A, Chryssanthopoulos MK. Elastic buckling and postbuckling behaviour of widely stiffened conical shells under axial compression. Eng Struct. 1999;21(9):845–855. https://doi.org/10.1016/S0141-0296(98)00043-4
31. Dubina D, Ungureanu V. Local/distortional and overall interactive buckling of thin-walled cold-formed steel columns with open cross-section. Thin-Walled Struct. 2023;182:110172. https://doi.org/10.1016/j.tws.2022.110172
32. Orloff KL, Rassati GA, Swanson JA, Burns TM. A study on the shear lag effects in longitudinally welded connections subject to eccentricity. ce/papers. 2021;4(2–4):900–907. https://doi.org/10.1002/cepa.1370
33. Quinn D, Murphy A, McEwan W, Lemaitre F. Stiffened panel stability behaviour and performance gains with plate prismatic sub-stiffening. Thin-Walled Struct. 2009;47(12):1457–1468. https://doi.org/10.1016/j.tws.2009.05.011
34. Hu Y, Yang J, Baniotopoulos C, Wang F. A comparison of structural performance enhancement of horizontally and vertically stiffened tubular steel wind turbine towers. Struct Eng Mech. 2020;73:1–14.
35. Ma W, Sun Z, Wu H, Xu L, Zeng Y, Wang Y, et al. Buckling analysis of thin-walled circular shells under local axial compression using vector form intrinsic finite element method. Metals. 2023;13:564. https://doi.org/10.3390/met13030564
36. Ghorbanpour Arani A, Loghman A, Barzoki A, Kolahchi R. Elastic buckling analysis of ring and stringer-stiffened cylindrical shells under general pressure and axial compression via the Ritz method. J Solid Mech. 2010; 2:1–12.
37. Evkin A, Krasovsky V, Lykhachova O, Marchenko V. Local buckling of axially compressed cylindrical shells with different boundary conditions. Thin-Walled Struct. 2019;141:374–388. https://doi.org/10.1016/j.tws.2019.04.024
38. Jiao P, Chen Z, Ma H, Ge P, Gu Y, Miao H. Buckling behaviors of thin-walled cylindrical shells under localized axial compression loads, part 2: numerical study. Thin-Walled Struct. 2021;169:108330. https://doi.org/10.1016/j.tws.2021.108330